Qubit State Monitoring by Measurement of Three Complementary Observables

Rusko Ruskov,[1,*] Alexander N. Korotkov,[2] and Klaus Mølmer[1]

[1]*Lundbeck Foundation Theoretical Center for Quantum System Research, Department of Physics and Astronomy, University of Aarhus, DK-8000 Aarhus C, Denmark*
[2]*Department of Electrical Engineering, University of California, Riverside, California 92521, USA*

We consider the evolution of a qubit (spin 1/2) under the simultaneous continuous measurement of three noncommuting qubit operators $\hat{\sigma}_x$, $\hat{\sigma}_y$, and $\hat{\sigma}_z$. For identical ideal detectors, the qubit state evolves by approaching a pure state with a random direction in the Bloch vector space and by undergoing locally isotropic diffusion in the perpendicular directions. The quantum state conditioned on the complete detector record is used to assess the fidelity of classically inspired estimates based on running time averages and discrete time bin detector outputs.

The needs of quantum computing and communication [1] are stimulating rapid progress in the control of single quantum systems. Recent experiments demonstrate coherent manipulation of quantum systems, including Rabi oscillations and entangling operations with few qubits. An important direction for advanced quantum control is to realize continuous monitoring of a quantum system. Theories of continuous quantum measurement [2–7] and experiments [8–11] have been carried out on a number of systems. Quantum monitoring can be used to prepare highly pure states and entangled states [4,12–16] and for continuous error correction [17].

A particularly interesting case is when noncommuting variables are being measured simultaneously. In Ref. [18], the signal cross correlation for two such detectors of an evolving qubit was calculated. In Ref. [19], Wei and Nazarov considered measurement outcomes for three detectors measuring a qubit in orthogonal directions. They analyzed the statistics of the integrated outcomes v_k for each detector and showed that if these outcomes happen to be sufficiently large, then the normalized vector $\boldsymbol{v}/|\boldsymbol{v}|$ is close to the Bloch vector of the actual qubit state.

In this Letter, we consider simultaneous continuous measurement of the qubit observables $\hat{\sigma}_x$, $\hat{\sigma}_y$, and $\hat{\sigma}_z$, illustrated in Fig. 1. The setup can be in principle realized with a trapped atom probed dispersively by optical cavity fields. In contrast to Ref. [19], we explicitly take into account the qubit evolution due to measurement and analyze the problem of monitoring the qubit state by using the measurement records. The three Pauli observables are complementary, but the incremental changes of the quantum state due to the weak measurements carried out in infinitesimal time intervals commute, and the simultaneous measurements contribute to purification of the quantum state 3 times faster than if only a single observable is measured. While the measurements drive the system towards the Bloch sphere surface (pure states), they cause locally isotropic diffusion in angular directions.

If the observer has access only to detector readout signals integrated over finite time intervals, the backactions associated with these accumulated signals do not commute, and the state of the qubit can only be approximately determined. The quality of the state estimate in this case is thus a measure of the role of complementarity of the observables detected. Comparing the exact qubit evolution with simple classically inspired ways of monitoring, we show that running averages with an exponential window can provide the fidelity of state monitoring up to 0.94. We also show that if the available measurement record is averaged over discrete time steps Δt, the monitoring fidelity decreases with Δt quite slowly.

Model.—We consider continuous measurement of the qubit observables $\hat{\sigma}_x$, $\hat{\sigma}_y$, and $\hat{\sigma}_z$ by three linear detectors with output signals $I_k(t)$. Let $u_k(t) = I_k(t) - I_{0,k}$, where $I_{0,k}$ denotes the uniform average of the outcomes of detector k over the two qubit states, and let Δu_k denote the detector responses, i.e., the difference of the mean signal for the qubit states. We can then write

$$u_k(t) = \frac{\Delta u_k}{2} \text{Tr}[\hat{\rho}(t)\hat{\sigma}_k] + \xi_k(t), \qquad k = x, y, z. \quad (1)$$

The $\text{Tr}[\hat{\rho}\hat{\sigma}_k]$ expectation values, determined by the time-dependent qubit density matrix $\hat{\rho}$, are in the following represented as the Bloch vector $\boldsymbol{r} = (x, y, z)$. In Eq. (1), $\xi_k(t)$ are independent white noises with one-sided spectral
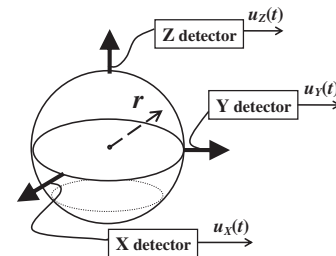
FIG. 1. A qubit measured by three orthogonal detectors.

densities S_k: $\langle \xi_k \xi_l dt \rangle = \delta_{kl} S_k/2$. The qubit evolution due to measurement by a linear detector (amplifier with infinite gain) can be described by three parameters [6,20]: the so-called measurement time $\tau_{\mathrm{meas},k} = 2S_k/(\Delta u_k)^2$, which determines the rate of quantum (informational) backaction, a factor K_k describing the classical backaction correlated with the output noise ξ_k, and an ensemble dephasing rate Γ_k, related to the single-qubit dephasing rate γ_k as $\Gamma_k = \gamma_k + 1/2\tau_{\mathrm{meas},k} + K_k^2 S_k/4$. In this Letter, we are interested in the quantum backaction due to measurements, and we assume the absence of classical backaction $K_k = 0$ as well as the absence of any Hamiltonian driving of the qubit.

If the measurement is performed by only one $\hat{\sigma}_k$ detector ($\Gamma_l = 0$ for $l \neq k$), then the probability density of its integrated result $\bar{u}_k(\tau) = \tau^{-1}\int_0^\tau u_k(t)dt$ is $P_{\mathrm{tot}}(\bar{u}_k) = \sum_i \rho_{ii}(0)P_i(\bar{u}_k)$, where the qubit density matrix $\hat{\rho}$ is written in the $\hat{\sigma}_k$ basis ($i = 1, 2$) and $P_i(\bar{u}_k) = \sqrt{\tau/\pi S_k}\exp\{-[\bar{u}_k + (-1)^i \Delta u_k/2]^2 \tau/S_k\}$ are the Gaussian distributions for the basis states. Then the qubit evolution is given by the Bayesian quantum filter [6]

$$\rho_{ij}(\tau) = \rho_{ij}(0)e^{-\gamma_k\tau(1-\delta_{ij})}\sqrt{P_i(\bar{u}_k)P_j(\bar{u}_k)}/P_{\mathrm{tot}}(\bar{u}_k). \quad (2)$$

In the case of three detectors measuring the qubit in the orthogonal bases, it is impossible to use the quantum Bayes rule for a finite τ because the measurement backactions do not commute. Therefore we should apply Eq. (2) in the differential form (for small dt) in the three orthogonal bases corresponding to the measured observables and then sum up the contributions to the qubit evolution. In this way we obtain the following equation in the Stratonovich form for the x component of the qubit Bloch vector $\mathbf{r}(t)$ given the measurement record $u_k(t)$:

$$\dot{x} = (1 - x^2)(\Delta u_x/S_x)u_x - xy(\Delta u_y/S_y)u_y$$
$$- xz(\Delta u_z/S_z)u_z - (\gamma_y + \gamma_z)x. \quad (3)$$

Evolution equations for the components y and z can be obtained by cyclic permutation of variables in Eq. (3).

Identical detectors.—In what follows we consider the case of three identical detectors: $\Delta u_k/S_k = \Delta u/S = a$ (we assume $a > 0$) and $\gamma_k = \gamma \geq 0$. Then the qubit evolution (3) can be rewritten in a vector form as

$$\dot{\mathbf{r}} = -2\gamma\mathbf{r} + a\{\mathbf{u}(1 - r^2) - [\mathbf{r} \times [\mathbf{r} \times \mathbf{u}]]\}, \quad (4)$$

where $\mathbf{u} \equiv (\Delta u/2)\mathbf{r} + \boldsymbol{\xi}(t)$ is the vector of results, Eq. (1), and $r = |\mathbf{r}|$. The evolution (4) is invariant under arbitrary rotations and can be represented as evolution due to one-detector measurement along a fluctuating random direction of $\mathbf{u}$. It is interesting to note that, while measurement of only single observable $\hat{\sigma}_k$ "attracts" the qubit state to one of the corresponding eigenvectors, the simultaneous measurement of $\hat{\sigma}_x$, $\hat{\sigma}_y$, and $\hat{\sigma}_z$ leads to no preferable direction in the Bloch space.

The ensemble-averaged evolution is also isotropic: $\dot{\mathbf{r}} = -2\Gamma\mathbf{r}$, which is easier to see from the Itô form [21] of (4):

$$\dot{\mathbf{r}} = -2\Gamma\mathbf{r} + a\{\boldsymbol{\xi}(1 - r^2) - [\mathbf{r} \times [\mathbf{r} \times \boldsymbol{\xi}]]\}, \quad (5)$$

where $\Gamma = \gamma + \Gamma_0$ is the one-detector ensemble decoherence and $\Gamma_0 = (\Delta u)^2/4S = 1/2\tau_{\mathrm{meas}}$. We also introduce the efficiency (ideality) of the measurement $\eta = \Gamma_0/\Gamma$.

Transforming Eq. (5) to polar coordinates, we obtain the following evolution for the radial component r:

$$\dot{r} = 2\Gamma_0(1/r - r/\eta) + a(1 - r^2)\xi_r, \quad (6)$$

where $\xi_r(t) = \mathbf{e}_r \cdot \boldsymbol{\xi}(t)$ is the noise component along $\mathbf{r}$ with the same spectral density: $\langle \xi_r \xi_r dt \rangle = S/2$. In directions perpendicular to $\mathbf{r}$, Eq. (5) leads to a locally isotropic Brownian diffusion with coefficient a; correspondingly, the angular evolution has the diffusion coefficient a/r (this can be shown by using locally geodesic coordinates).

In particular, for an ideal measurement ($\eta = 1$) and a pure initial state, the state remains pure [$r = 1$; see Eq. (6)] and the diffusion on the Bloch sphere can be described by the Fokker-Planck (FP) equation $\partial p(\theta, \varphi)/\partial t = \Gamma_0 \Delta_{\theta,\varphi} p(\theta, \varphi)$, where $\Delta_{\theta,\varphi}$ is the angular part of the Laplacian. The solution of this equation [22] at time τ is $p(\Theta; \tau) = \sum_{n=0}^\infty \frac{2n+1}{4\pi} e^{-n(n+1)V/4} P_n(\cos\Theta)$, where Θ is the angle from the initial state, $P_n(z)$ are the Legendre polynomials, and $V = 4\Gamma_0\tau = 2\tau/\tau_{\mathrm{meas}}$ is the variance. Obviously, for $\tau \gg \tau_{\mathrm{meas}}$ the initial state is forgotten, and the distribution $p(\Theta; \tau) \to 1/4\pi$ becomes isotropic. We note that, while the average state approaches the center of the Bloch sphere, the actual monitored qubit state remains pure, performing a random walk on the sphere.

Purification dynamics.—We characterize state purity by $\mathcal{P} \equiv 2\,\mathrm{Tr}\hat{\rho}^2 - 1 = r^2$. For an ideal measurement $\eta = 1$, and starting from a nonpure initial state, the qubit will purify ($\mathcal{P} \to 1$) on a time scale of the order of τ_{meas}. For a nonideal measurement $\eta < 1$, purity will continue to fluctuate around a stationary average value $\langle \mathcal{P} \rangle_{\mathrm{st}} < 1$.

To analyze the purification dynamics we use Eq. (6) to derive the Itô equation for the purity: $d\mathcal{P}/dt = 2\Gamma_0[2(1 - \mathcal{P}/\eta) + (1 - \mathcal{P})^2] + 2a(1 - \mathcal{P})\sqrt{\mathcal{P}}\xi_r(t)$. The corresponding FP equation [21] is $\frac{\partial p(\mathcal{P},t)}{\partial t} = -\frac{\partial}{\partial \mathcal{P}} \times [A(\mathcal{P})p(\mathcal{P}, t)] + \frac{1}{2}\frac{\partial^2}{\partial \mathcal{P}^2}[B(\mathcal{P})p(\mathcal{P}, t)]$ with coefficients $A(\mathcal{P}) = 2\Gamma_0[2(1 - \mathcal{P}/\eta) + (1 - \mathcal{P})^2]$, $B(\mathcal{P}) = 8\Gamma_0\mathcal{P}(1 - \mathcal{P})^2$, and initial distribution $p(\mathcal{P}, 0) = \delta(\mathcal{P} - \mathcal{P}_0)$. At $t \gg \tau_{\mathrm{meas}}$ the purity reaches a stationary distribution

$$p_{\mathrm{st}}(\mathcal{P}, \eta) = N^{-1}\frac{\sqrt{\mathcal{P}}}{(1 - \mathcal{P})^3}\exp\left[-\frac{\mathcal{P}(1 - \eta)}{(1 - \mathcal{P})\eta}\right], \quad (7)$$

where N is the normalization. For $\eta \to 1$, $p_{\mathrm{st}}(\mathcal{P}, \eta)$ approaches the δ function at $\mathcal{P} = 1$.

In Fig. 2, we show the average purity (solid lines) $\langle \mathcal{P} \rangle_{\mathrm{FP}}(t) = \int_0^1 \mathcal{P}p(\mathcal{P}, t)d\mathcal{P}$ for measurement efficiencies $\eta = 1$, 0.5, and 0.1, calculated by numerically solving the FP equation starting from the Bloch sphere center ($\mathcal{P}_0 = 0$). The FP distribution $p(\mathcal{P}, t)$ (not shown) has been also confirmed by the simulations using Eq. (4).
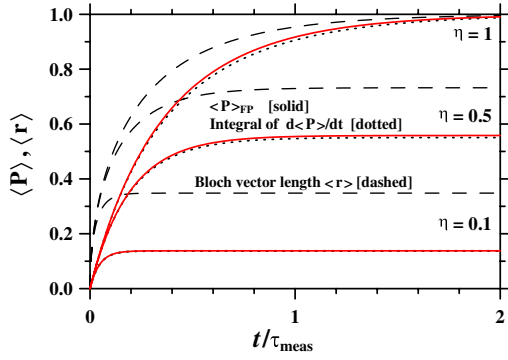
FIG. 2 (color online). Solid lines: Averaged purity evolution $\langle \mathcal{P} \rangle_{\mathrm{FP}}(t)$ starting from the fully mixed state. Dotted lines: The same evolution integrating Eq. (8). Dashed lines: Evolution of $\langle r \rangle = \langle \sqrt{\mathcal{P}} \rangle_{\mathrm{FP}}$.

The purification dynamics can be approximated by using the ensemble-averaged purification rate [13,14] obtained from the above Itô equation, starting from a given purity:

$$\langle d\mathcal{P} \rangle / dt = 2\Gamma_0 [2(1 - \mathcal{P}/\eta) + (1 - \mathcal{P})^2]. \quad (8)$$

For ideal detectors ($\eta = 1$) this becomes $2\Gamma_0(1 - \mathcal{P}) \times (3 - \mathcal{P})$, which can also be easily obtained from the purification result [13,23] $\langle d\mathcal{P} \rangle / dt = 2\Gamma_0(1 - \mathcal{P})(1 - z^2)$ for a z detector by adding the contributions from measurements in the x and y directions, so that $1 - z^2 \rightarrow 3 - r^2$. The purification by three detectors is isotropic, and its rate $\langle d\mathcal{P} \rangle / dt$ is therefore 3 times faster than for a single detector averaged over random directions in the Bloch space. This may be compared with the result of adaptive measurements with a single detector, perpendicular to the current Bloch vector estimate, which leads to the fastest purification [13,14]. The performance of nonadaptive switching between random bases is addressed in Ref. [16] including an analysis of the purification speedup as a function of Hilbert space dimension. It is important to note that the average purity $\langle \mathcal{P} \rangle_{\mathrm{FP}}(t)$ differs from the naive integration of Eq. (8) (dotted lines in Fig. 2) because $\langle d\mathcal{P} \rangle \neq d\langle \mathcal{P} \rangle$ and the purity distribution $p(\mathcal{P}, t)$ is generally different from the δ function. In particular, $\langle \mathcal{P} \rangle_{\mathrm{st}}$ is slightly higher (for $\eta \neq 0, 1$) than the stationary value $(1 + 1/\eta) - \sqrt{(1 + 1/\eta)^2 - 3}$ derived from Eq. (8).

Classically inspired state monitoring.—Exact monitoring of the qubit state is realized by integrating the evolution equation (4) given the measurement record $u_k(t)$. However, such real-time computation may be a challenge experimentally, and therefore it is interesting to analyze the fidelity of simplified signal processing algorithms. To decrease the noise component and reduce the bandwidth of signals given by Eq. (1), it is natural to average them over a running time window: $\tilde{u}_k(t) \equiv \int_{-\infty}^t g(t - t') u_k(t') dt'$, where $g(\Delta t)$ is the window profile. We have considered (i) a rectangular window of duration τ: $g(\Delta t) = \tau^{-1}$ for $\Delta t < \tau$ and zero otherwise and (ii) an exponential window with decay time τ: $g(\Delta t) = \tau^{-1} \exp(-\Delta t / \tau)$. The

analyzed monitoring algorithm is very simple: At any t in the stationary regime ($t \gg \tau, \tau_{\mathrm{meas}}$) we estimate the qubit state as the pure state $r_{\mathrm{est}}(t) = \tilde{u}(t)/|\tilde{u}(t)|$. The algorithm fidelity is defined as the time-averaged scalar product of this vector with the actual state $r(t)$:

$$F \equiv 2\langle \mathrm{Tr} \hat{\rho}_{\mathrm{est}} \hat{\rho} \rangle_t - 1 = \langle r \cdot \tilde{u}/|\tilde{u}| \rangle_t. \quad (9)$$

In Fig. 3, we show the fidelity F vs the window duration τ for the rectangular (solid lines) and exponential (dashed lines) windows, calculated by simulating the evolution (4) for $\eta = 1$, 0.5, and 0.1. For $\eta = 1$ the fidelity reaches a maximum of $F_{\max} = 0.94$ for the exponential window with $\tau = 0.6\tau_{\mathrm{meas}}$ (for the rectangular window $F_{\max} = 0.87$ at $\tau = 0.9\tau_{\mathrm{meas}}$). For small τ the fidelity is suppressed due to large fluctuations: $|\tilde{u}| \sim \tau^{-1/2}$, while for $\tau \gtrsim \eta\tau_{\mathrm{meas}}$ it decreases because signals from the distant past lose their relevance to $r(t)$. To analyze the latter effect quantitatively, we have used Eq. (4) to find the signal-qubit correlations: $\langle u_z(t - \Delta t) z(t) \rangle = (\Delta u/2) \exp(-\Delta t / \eta\tau_{\mathrm{meas}})$, $\langle u_z(t - \Delta t) x(t) \rangle = \langle u_z(t - \Delta t) y(t) \rangle = 0$ [24].

Since $F = \langle r \cos\phi \rangle_t$, where ϕ is the angle between $\tilde{u}$ and r, the fidelity is bounded from above by the stationary Bloch vector length $\langle r \rangle$ reached at $t \rightarrow \infty$ (Fig. 2, dashed lines). In Fig. 3, these bounds are shown as horizontal lines: $\langle r \rangle = 0.732$ for $\eta = 0.5$ and $\langle r \rangle = 0.348$ for $\eta = 0.1$ (obviously, $\langle r \rangle = 1$ for $\eta = 1$). It is interesting to see that with decreasing η, the exponential window $F_{\max}$ approaches $\langle r \rangle$. This means that at optimal τ either $\tilde{u}$ becomes practically aligned with r, $\langle \cos\phi \rangle_t \rightarrow 1$, or there is a significant correlation between fluctuations of $r(t)$ and $\phi(t)$. This correlation can be checked by comparing F with the uncorrelated value $\langle r \rangle \langle \cos\phi \rangle_t$ shown in Fig. 3 by dotted lines. We see practically no correlation at the optimal point for small η, which means that $\langle \cos\phi \rangle_t \rightarrow 1$.

Algorithms for time-discretized data.—We consider now a situation when only the integrated detector signals $u_k^{(n)} \equiv \frac{1}{\Delta t} \int_{t_n - \Delta t}^{t_n} u_k(t') dt'$ are available at discrete time moments $t_n = n\Delta t$, $n = 0, 1, \ldots$, as in the experiment [10].
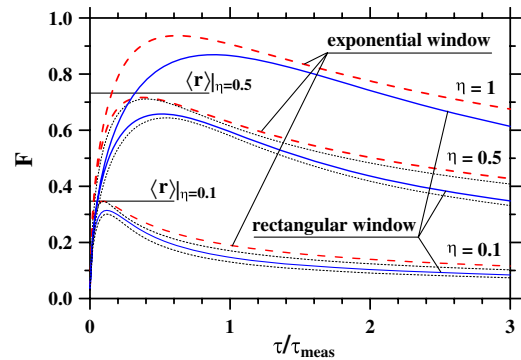
FIG. 3 (color online). Monitoring fidelity (9) vs window duration τ for the rectangular (solid lines) and exponential windows (dashed lines). Dotted lines show the uncorrelated product $\langle r \rangle \langle \cos\phi \rangle_t$.
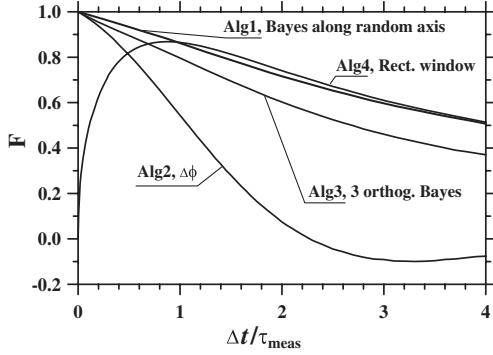
FIG. 4.   Monitoring fidelity vs time step Δt for four algorithms processing time-discretized detector data (see text).

Assuming ideal detectors to deal with pure states only, we have studied four algorithms, which output estimated states r_{est} at moments t_n, and calculated their fidelities (shown in Fig. 4) defined as $F = \langle r \cdot r_{est} \rangle_n$, similar to Eq. (9) but with averaging over moments t_n. The actual evolution $r(t)$ in this case is simulated via Eq. (4), and we have checked that the fidelity does not depend on the inaccuracy of the initial state estimate. Algorithm 1 treats the vector of measurement data $u^{(n)}$ as a single measurement of the spin component along this vector and updates the qubit state using the quantum Bayes rule (2) in the corresponding basis, changing at each time step. For small Δt the fidelity of this algorithm is $F \approx 1 - 0.14 \Delta t / \tau_{meas}$. Somewhat unexpectedly, even for $\Delta t \simeq \tau_{meas}$ the fidelity is still quite good. Algorithm 2 at each step rotates the previous Bloch vector $r(t_{n-1})$ towards the vector $u^{(n)}$ by the angle $\Delta\phi = (\Delta u / S) u_\perp^{(n)} \Delta t$, which is determined by the component $u_\perp^{(n)}$ of the vector $u^{(n)}$ perpendicular to $r(t_{n-1})$. Even though for small Δt this is very similar to Algorithm 1, the fidelity decreases more rapidly with increasing Δt. Algorithm 3 treats the three measurement outcomes as the results of sequential measurements of the three spin components and uses the Bayesian update rule accordingly. For $\Delta t \to 0$ the fidelities of all three algorithms approach unity, though with different slopes. Algorithm 4 treats the data available at moments t_n in the same way as the running rectangular window (see the upper solid line in Fig. 3) and estimates the state as $u^{(n)} / |u^{(n)}|$. Algorithm 4 suffers from large statistical errors for short Δt; however, for $\Delta t \approx \tau_{meas}$ the fidelities of Algorithms 1 and 4 become practically equal, and for longer Δt Algorithm 4 becomes the best among considered algorithms.

In conclusion, state monitoring and purification by simultaneous measurements of noncommuting observables has been described by a quantum filtering theory. The shortcomings of simple, effective algorithms reflect the difficulty of estimating quantum states from incomplete measurement data. The incompleteness of the time-averaged or integrated data is due to complementarity and the noncommuting backaction operations in the coarse-grained limit of finite sampling times. Our analysis shows this very clearly, and it quantifies the approach to perfect state estimation in the limit of continuous measurement and quantum filtering.

*On leave from INRNE, Sofia BG-1784, Bulgaria.

[1]   M. A. Nielsen and I. L. Chuang, *Quantum Computation and Quantum Information* (Cambridge University Press, Cambridge, England, 2000).

[2]   V. P. Belavkin and P. Staszewski, Phys. Lett. A **140**, 359 (1989).

[3]   H. J. Carmichael, *An Open System Approach to Quantum Optics* (Springer, Berlin, 1993).

[4]   H. M. Wiseman and G. J. Milburn, Phys. Rev. Lett. **70**, 548 (1993); Phys. Rev. A **49**, 1350 (1994).

[5]   J. Dalibard, Y. Castin, and K. Mølmer, Phys. Rev. Lett. **68**, 580 (1992).

[6]   A. N. Korotkov, Phys. Rev. B **63**, 115403 (2001).

[7]   R. Ruskov, A. N. Korotkov, and A. Mizel, Phys. Rev. Lett. **96**, 200404 (2006).

[8]   N. Katz *et al.*, Science **312**, 1498 (2006); Phys. Rev. Lett. **101**, 200401 (2008).

[9]   S. Gleyzes *et al.*, Nature (London) **446**, 297 (2007).

[10] A. Palacios-Laloy *et al.*, Nature Phys. **6**, 442 (2010).

[11] J. E. Reiner *et al.*, Phys. Rev. A **70**, 023819 (2004).

[12] R. Ruskov and A. N. Korotkov, Phys. Rev. B **66**, 041401 (R) (2002); **67**, 241305(R) (2003).

[13] K. Jacobs, Phys. Rev. A **67**, 030301(R) (2003); J. Combes and K. Jacobs, Phys. Rev. Lett. **96**, 010504 (2006).

[14] H. M. Wiseman and J. F. Ralph, New J. Phys. **8**, 90 (2006).

[15] A. Negretti, U. V. Poulsen, and K. Mølmer, Phys. Rev. Lett. **99**, 223601 (2007).

[16] J. Combes, H. M. Wiseman, and A. J. Scott, Phys. Rev. A **81**, 020301(R) (2010).

[17] C. Ahn, H. M. Wiseman, and G. J. Milburn, Phys. Rev. A **67**, 052310 (2003).

[18] A. N. Jordan and M. Büttiker, Phys. Rev. Lett. **95**, 220401 (2005).

[19] H.-D. Wei and Yu. V. Nazarov, Phys. Rev. B **78**, 045308 (2008).

[20] A. A. Clerk *et al.*, Rev. Mod. Phys. **82**, 1155 (2010).

[21] C. W. Gardiner, *Handbook of Stochastic Methods* (Springer, Berlin, 1983).

[22] F. Perrin, C. R. Acad. Sci. Paris Ser. IV **181**, 514 (1925); P. H. Roberts and H. D. Ursell, Phil. Trans. R. Soc. A **252**, 317 (1960).

[23] A. N. Jordan and A. N. Korotkov, Phys. Rev. B **74**, 085307 (2006).

[24] The cross correlators vanish since $\langle xy \rangle = \langle xz \rangle = \langle yz \rangle = 0$ from symmetry, while correlators like $\langle u_z(t - \Delta t) z(t) \rangle$ have two contributions: $\langle z(t - \Delta t) z(t) \rangle = \frac{1}{3} \exp(-2\Gamma\Delta t)$ and $\langle \xi_z(t - \Delta t) z(t) \rangle = \frac{\Delta u}{3} \exp(-2\Gamma\Delta t)$.